

Review

Near-Infrared Fluorescent Nanoprobes for *in Vivo* Optical Imaging

Chai-Hoon Quek¹ and Kam W. Leong^{1,2,*}

¹ Department of Mechanical Engineering and Materials Science, Duke University, Durham, NC 27708, USA; E-Mail: cq4@duke.edu

² Department of Biomedical Engineering, Duke University, Durham, NC 27708, USA

* Author to whom correspondence should be addressed; E-Mail: kam.leong@duke.edu; Tel.: +1-919-660-8466; Fax: +1-919-684-4488.

Received: 9 January 2012; in revised form: 23 February 2012 / Accepted: 26 March 2012 /

Published: 30 March 2012

Abstract: Near-infrared (NIR) fluorescent probes offer advantages of high photon penetration, reduced light scattering and minimal autofluorescence from living tissues, rendering them valuable for noninvasive mapping of molecular events, assessment of therapeutic efficacy, and monitoring of disease progression in animal models. This review provides an overview of the recent development of the design and optical property of the different classes of NIR fluorescent nanoprobes associated with *in vivo* imaging applications.

Keywords: near-infrared; *in vivo* imaging; fluorescent dyes; nanotechnology; nanoprobes

1. Introduction

The first medical imaging was realized in the late 1895 by Wilhelm Röntgen shortly after he discovered X-ray and applied to capturing the images of the bones of a hand on film [1]. The immediate consequence of this discovery triggered intense development of new imaging technologies, such as X-ray computed tomography, magnetic resonance imaging, positron emission tomography, ultrasound and optical imaging, that are indispensable to diagnostic medicine (Table 1) [2,3]. These imaging technologies differ predominantly in the following aspects: resolution, penetration depth, temporal resolution and energy expended for generation of the image.

Today, these modern imaging technologies coupled with newly developed imaging probes are widely used in monitoring disease progression, interrogating cellular and molecular events, evaluating safety and toxicology in drug discovery and development, and assessing therapeutic efficacy *in vivo* [2,4–12].

Among the different imaging modalities, optical imaging, which owes its origin to single-cell *in vitro* studies, is attractive for small animal imaging because of its lower cost, portability, and potentially high spatial resolution with customizable fine-tuning. Despite being one of the most attractive techniques to provide noninvasive and nonionizing *in vivo* visualization [13], optical imaging is impeded by the tendency of living biological tissues to absorb and scatter photons and generate strong autofluorescence, which interferes with signal collection and processing (Figure 1) [14]. In addition, living tissues also contain other major NIR absorbers, such as water, lipids oxyhemoglobin and deoxyhemoglobin [5] that prove challenging for optical imaging. To overcome these barriers, intense research has focused on developing highly sensitive and efficient fluorescent probes that function in the biologically transparent window of the first and second NIR region (NIR I, 650–950 nm, and NIR II, 1000–1350 nm) (Figure 2) [15]. This review will provide a broad overview of the available NIR fluorescent probes, their optical properties and potential applications for *in vivo* imaging.

Table 1. Overview of imaging systems for small animals.

Modality	Resolution	Depth	Optimal use	Signal	Training/ expertise required	Cost ⁺
MRI	10–100 μm	No limit	Anatomical assessment, investigation of physiological, metabolic, molecular and genetic events.	RF * waves (Nonionizing radiation)	Yes (Certified radiologists)	\$\$\$
PET	0.8–1.4 mm	No limit	Investigation of physiological, metabolic, molecular and genetic events.	γ -rays (Ionizing radiation)	Yes (Certified radiologists)	\$\$\$
SPECT	0.8–1.4 mm	No limit	Investigation of physiological, metabolic, molecular and genetic events.	γ -rays (Ionizing radiation)	Yes (Certified radiologists)	\$\$
CT	50 μm	No limit	Anatomical assessment.	X-ray (Ionizing radiation)	Yes (Certified radiologists)	\$\$
Ultrasound	50 μm	mm	Anatomical assessment, investigation of physiological, metabolic, molecular and genetic events.	Sound waves (Nonionizing radiation)	Yes (Certified sonographers)	\$\$
Fluorescence optical imaging	0.3 μm	<1 cm	Metabolic, molecular and genetic events.	Light waves (Nonionizing radiation)	No	\$

MRI, Magnetic resonance imaging; PET, Positron emission tomography; SPECT, Single photon emission computed tomography; CT, Computed tomography. * RF, radiofrequency, ⁺ Cost of system: \$ < 100,000; \$\$ 100–300,000; \$\$\$ 1–3 millions.

Figure 1. Wavelength-dependent autofluorescence of vital organs and body fluids. (a) Image of the viscera of an athymic nude mouse taken immediately after sacrifice. The arrows indicate the location of gall bladder (GB), small intestine (SI) and bladder (BI). Tissue autofluorescence was imaged using three different excitation/emission filter sets; (b) blue/green (460–500 nm/505–560 nm); (c) green/red (525–555 nm/590–650 nm); and (d) Near-infrared (NIR) (725–775 nm/790–830 nm). (Reprinted with permission from [14], copyright 2003 Elsevier).

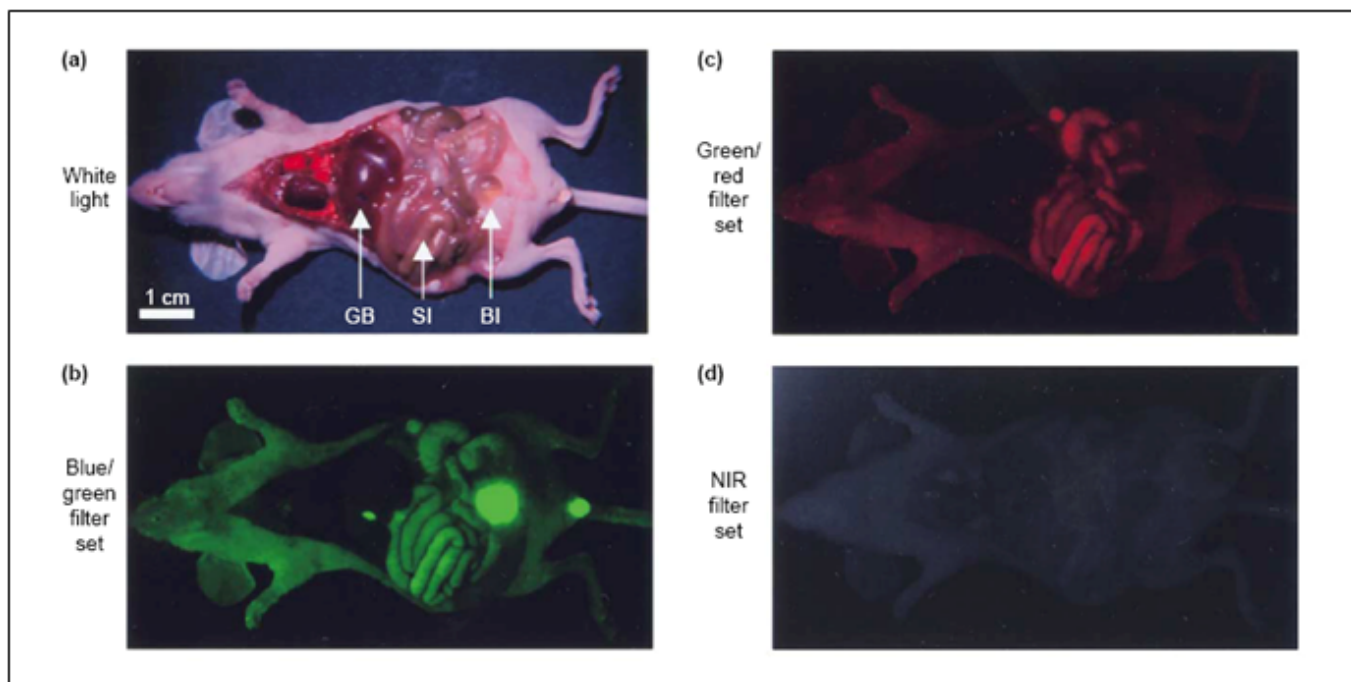
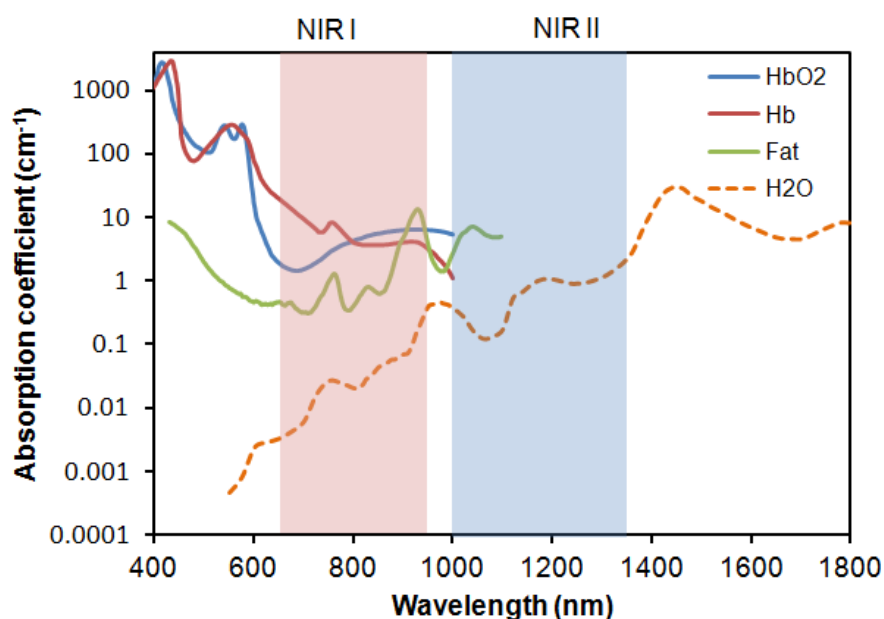


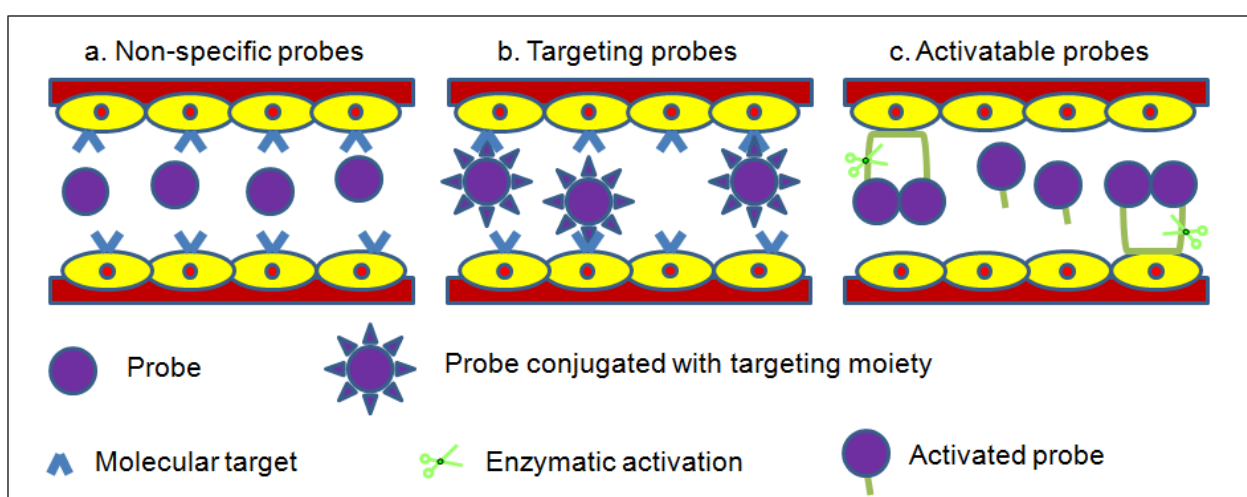
Figure 2. Absorption coefficient (on a log scale) of oxygenated blood, deoxygenated blood, fatty tissue and water as a function of wavelength.



2. Labeling Mechanism of Fluorescent Probes

Optical imaging has increasingly been used for dynamic noninvasive imaging of biological events in mouse models. Due to the lack of NIR fluorescence contrast generated by most tissues in the biological transparency window, exogenous fluorescent probes have to be administered for *in vivo* studies in order to visualize living tissues in its native physiological state. Ideally, the fluorescent probes to be administered should be biologically stable in the *in vivo* environment, and accumulate and produce imaging contrast at the target site. Fluorescent probes are classified according to their mechanism of contrast generation, collectively as non-specific, targeting and activatable (Figure 3) [6].

Figure 3. Modes of contrast generation of fluorescent probes. (a) Non-specific compartmental distribution of the probes. (b) Targeted binding of probes via surface ligands to molecular targets. (c) Activatable probes quenched in their native state and become fluorescent by enzyme-mediated cleavage.



Non-specific probes simply have differential distribution and are used to assess physiological processes such as changes in blood volume, permeability and perfusion in angiogenesis (Figure 3a). Typically, they achieve only low target-to-background signals due to the non-binding circulating probes producing significant background fluorescence within the compartment.

Tissue- or cell-specific contrast is created by coupling a targeting moiety to a fluorescent probe that binds specifically to a receptor thus generating the readout signal (Figure 3b). These probes can report more detailed information about the biological events than non-specific probes. Targeting probes can achieve high target-to-background signals provided the targeting moiety has a high affinity for the receptor and any unbound probes are thoroughly removed from the system, thereby reducing the background fluorescence.

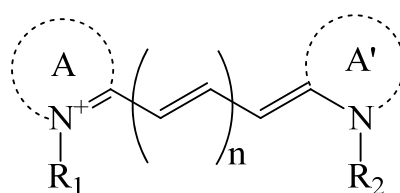
Activatable probes comprise of donor-acceptor fluorophores that are coupled to each other in close proximity to maintain a quenched state (Figure 3c). The fluorescence emission is activated by enzyme-mediated cleavage that releases the fluorescent probes. Activatable probes can attain high target-to-background signals as these probes in their native injected state are relatively undetectable.

3. Small Organic Fluorophores

3.1. Non-Specific Organic-Dye Probes

The choice of a suitable dye for *in vivo* imaging depends on many factors. The most important consideration would be the molar extinction coefficient and quantum yield of the dye in the NIR region [16,17]. Of all the dyes, cyanine makes up the majority of commercial fluorescent probes for *in vivo* applications. Cyanine is a synthetic dye family of the polymethine group with a conjugated chain of odd number of carbon atoms linked between two nitrogen centers (Figure 4) [18]. Among this class of compounds, carbocyanine dyes with indolic groups are readily available commercially and have also been synthesized in a large variety of analogues. The structure of carbocyanine is formed by reaction of two indolic isomers (either identical or different) linked on each end of a C1, C3 or C5 methine. The absorption and fluorescence emission wavelength is determined both by the chain length of the methine and the side chains attached to the indolic groups. Table 2 shows a series of commercially available carbocyanine dyes emitting in the visible to NIR range. These dyes generally exhibit high molar extinction coefficients but only have moderate fluorescence quantum yields up to 30%. A prominent representative of the NIR cyanine dye is Indocyanine green (ICG). ICG was first synthesized in the fifties [19] and is the only clinically approved dye available commercially. It has been used in optical imaging of changes in blood-brain barrier permeability after thrombus formation in a mouse model of cerebral venous thrombosis [20] and liver perfusion in mouse [21]. Clinically, ICG has been used in clinical retinal angiography [22], hepatic function testing [23] and imaging of human brain [24,25]. Since ICG binds tightly to plasma proteins and becomes confined to the vascular system, they are widely used for intraoperative assessment of vascular flow in cardiovascular surgery [26–28]. Because of its amphiphilicity and a shortage of functional groups available for conjugation, ICG could only function as a non-specific probe for *in vivo* imaging.

Figure 4. Generalized structure of cyanine dyes. A and A' are two quaternized heteroaromatic bases.

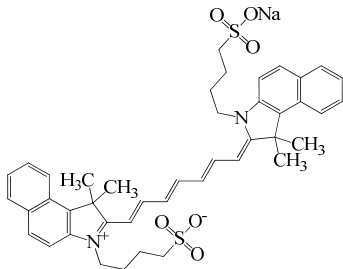
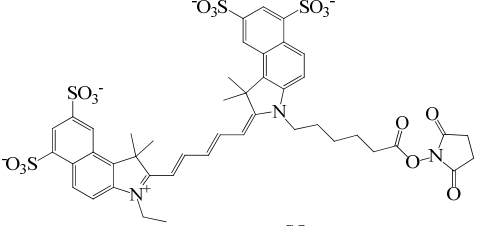
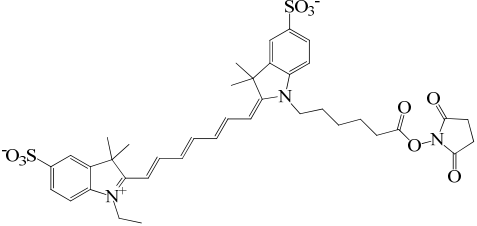
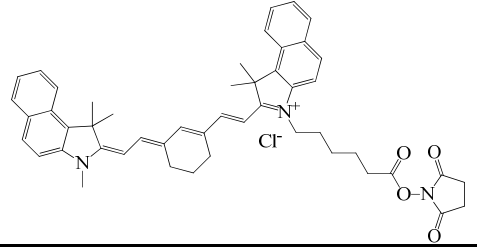


3.2. Targeting Organic-Dye Probes

Covalent attachment of targeting moieties such as antibodies, antibody fragments, proteins and peptides to fluorescent dyes can significantly improve the target-to-background signal. The strategy of conjugating antibodies to cyanine dyes were first demonstrated by Folli *et al.* and Ballou *et al.* [29,30] and applied to fluorescence imaging of tumor in mice. Antibodies, however, have found limited utility due to their unfavorable pharmacokinetics. The typical circulating half-life of antibodies is much shorter than the time required to access a small tumor with reasonable accumulation, thus rendering effective targeting rare using antibodies [31].

To improve the pharmacokinetics of *in vivo* contrast agents, a possible approach is to reduce the conjugate molecular size while still preserving the targeting affinity of the labeled dyes. Neri *et al.* demonstrated this idea by conjugating antibody single chain fragments selected from phage display libraries against an angiogenesis-associated oncofetal fibronectin isoform to cyanine dyes and applied to imaging of angiogenesis in a variety of animal models [32,33]. Alternative strategy is also shown in the work by Achilefu *et al.* and Licha *et al.* highlighting the successful application of receptor-specific peptide-dye conjugates for fluorescent imaging of tumors [34–36]. As a whole, fluorescent dyes can be readily functionalized to achieve targeting.

Table 2. Structures and optical characteristics of commercial NIR cyanine dyes.

Dye	Structure	Abs/Em (nm)	Molar extinction coefficient ($M^{-1} cm^{-1}$)	Quantum yield
Indo-Cyanine Green (ICG) [17]		807/822	121,000	0.09
Cy5.5 NHS ester *		675/694	250,000	0.23
Cy7 NHS ester *		747/774	200,000	0.28
Cy7.5 NHS ester §		788/808	223,000	N.A.

* Information is obtained from supplier GE Healthcare website; § Information is obtained from supplier Lumiprobe website.

3.3. Activatable Organic-Dye Probes

The concept of activatable NIR probes was introduced by Weissleder *et al.* for *in vivo* imaging of enzyme activity [37]. Enzyme-activatable probes contain either two identical or different fluorophores linked in close proximity to each other by a specific peptide linker. The fluorescence of the probes is

essentially undetectable in the quenched state. After enzymatic cleavage, the fluorophores are separated to restore the fluorescence emission. A large number of activatable probes have been documented, among them the enzyme activation of NIR targeting dyes is mediated mainly by tumor associated proteases, such as cathepsins, caspases and matrix metalloproteinases [38–43]. The ability of activatable fluorescent probes to detect gene expression is particularly useful as a means to diagnose malignant molecular process in the early disease state [44].

4. Nanomaterial-Based Fluorescent Probes

Despite the long history of *in vivo* optical imaging, organic dyes have suffered from small Stokes shifts, poor photostability, high plasma protein binding rate, aggregation and background fluorescence in aqueous medium [45]. Attention has been increasingly channeled toward nanotechnology to search for new class of more effective probes. Many nanomaterials are already widely used as catalysts, and energy storage and electronic devices [46–50]. Their application to the biomedical arena has attracted a similarly enthusiastic following. Interest in the nanomaterials arises from the fact that at nanoscale the properties of materials can be very different from their bulk counterparts. Firstly, nanomaterials when compared to the same mass of material existing in a larger form have a much higher surface area. As such, nanomaterials are more chemically reactive because of the high surface energy. In addition, at nanoscale range, quantum effects begin to dominate the behavior of matter, affecting the optical, electrical and magnetic behavior of materials [51,52].

Lately, the integration of nanotechnology with medicine has found many novel applications of nanomaterials. Nanoparticles can be engineered to overcome biological barriers for effective and targeted delivery of drugs, genes, and contrast agents [53]. Active moieties such as proteins, peptides and nucleic acids can easily be conjugated to the surface of the nanoparticles for use as non-specific, targeting or activatable nanoprobe. The following sections are devoted to the recent development of some particulate NIR fluorescent nanoprobe for potential *in vivo* imaging.

4.1. Quantum Dots

Fundamentally, quantum dots (QDs) are semiconductor nanocrystals that absorb photons of light and re-emit photons at a different wavelength (Figure 5a) [54]. Typically, QDs are of ~2–20 nm in diameter depending on the core composition and the surface coating or functionalization. Most of the QDs reported have a core/shell structure (Figure 5b) with the core composed of atoms from periodic groups II–VI (CdSe, CdTe, CdS, PbSe, ZnS and ZnSe), III–V (GaAs, GaN, InP, InAs), and IV–VI (PbS). QDs differ from traditional organic fluorescent dyes and naturally fluorescent proteins in several important aspects. Firstly, QDs are extremely efficient in generating fluorescence, often by an order of magnitude higher than traditional fluorophores. In addition, QDs fluoresce without involving conjugated double-bond systems, thus exhibit greater photostability to enable long-term imaging without the concern of photo-induced deterioration. Another practical advantage of QDs is that their emission spectra are narrow and symmetric, thus minimizing any overlapping of colors in multi-component imaging applications. With the same underlying material, varying the size of the QDs could give rise to different emission peaks, giving QDs unprecedented tunability. This enables the use of a single laser to excite and achieve multicolor emission for multiplexed assays [53,55–57]. These unique properties of QDs have

been increasingly exploited as bioimaging agents [58–61], theranostic platforms to deliver and track siRNA-based therapy [62–65], nanosensors to study intracellular trafficking and unpacking of DNA nanocomplexes [66–69], and cell lineage-tracing agents to follow the development of stem and progenitor cells *in vivo* developmental [70,71].

For *in vivo* imaging, the fluorescent emission wavelengths of the QDs ideally should be around 700–1000 nm, in the NIR region to minimize the endogenous fluorescence and the interference from major absorbers in the body. As presented in Figure 5a, CdTe [72,73], CdTe/CdSe [74], CdHgTe/ZnS [75,76], InAs [77], InAs_xP_{1-x}/InP/ZnSe [78], and PbSe [79,80] are the possible QDs that emit in the NIR I region. All these QDs are usually passivated with a layer of ZnS or ZnSe to protect the core from oxidation and to prevent the leaching of toxic heavy metal ions such as Cd, Hg, As and Pb into the surrounding solution. However, with the several reports indicating Cd-containing QDs showing cytotoxicity under extreme conditions [81–85], there is a rising concern of using them for long term *in vivo* applications. Therefore, attention has been channeled to develop new class of quantum dots comprising of less-toxic elements. Some of these newly developed NIR QDs include Cu-doped InP/ZnSe [86], CuInSe [87,88], and CuInS₂/ZnS [12,89,90].

Among the synthetic routes of QDs, the most commonly used technique is to first generate the core by injecting liquid precursors into nonpolar coordinating organic solvent at a temperature as high as 300 °C and subsequently growing the shell layer of ZnS onto the core [54,56,91,92]. QDs generated by this method are by default hydrophobic and are unsuitable for use in biological systems. To render them dispersible in aqueous medium, the QDs such as CuInS₂/ZnS are transferred into aqueous phase either by ligand exchange with dihydrolipoic acid/polyethylene glycol 1000 (DHLAPEG100) or by encapsulation in phospholipid micelles [60,90,93,94]. The resulting water-soluble QDs emit at wavelength greater than 700 nm and could achieve good quantum yield of 30%. *In vivo* sentinel lymph node imaging with the CuInS₂/ZnS QDs were performed in the work of Pons *et al.* by subcutaneous injection into regional lymph nodes (LN) of healthy mice. It was observed that the QDs preferentially accumulated at the injection site, in the two regional LNs and to a lesser extent in other organs over a 10-day observation period [95]. The results suggest that the LNs would be more sensitive toward acute QD toxicity. They further compared the inflammatory response of the two regional LNs treated with CuInS₂/ZnS and CdTeSe/CdZnS QDs. Histological sections indicated inflammation only occurred at 10 times dose concentration for cadmium-free QDs than for the Cd-containing counterparts (Figure 5c,d). This study highlights the advantage of cadmium-free QDs for safer NIR *in vivo* imaging.

4.2. Colloidal Silicon Quantum Dots

Silicon is one element that is most widely used in the microelectronics industry due to its outstanding performance as an electronic material [96,97]. Its inherit nontoxic and environmentally friendly characteristic has attracted much attention to develop silicon quantum dots (Si QDs) for biological applications [98–101]. An important step toward realizing these applications is the fabrication of colloiddally and optically stable, water-dispersible Si QDs. Silicon QDs are typically prepared in a two-step process: first by CO₂ laser pyrolysis of silane to generate non-photoluminescent crystalline Si particles with an average diameter of 5 nm [102]. Etching with mixture of hydrofluoric acid and nitric acid is then followed to reduce the size and passivate the surface of the particles [103]. Using this method Si QDs with size ranging from 1 to 5 nm and emission from blue to NIR can be obtained.

In 2004, Li *et al.* first demonstrated the potential of Si QDs for biological applications. They grafted water-soluble polyacrylic acid Si QDs to label Chinese hamster ovary (CHO) cells for *in vitro* imaging [104]. In the recent work by Park *et al.* they delivered Si QDs loaded with anti-cancer drug doxorubicin D-LPSiNPs into BALB/c mice and monitored both accumulation and degradation *in vivo* (Figure 6) [99]. Si QDs are exhibiting the attractive attributes to be an effective and biocompatible nanomaterials system for theranostic purpose; they will undoubtedly see intense effort for further improvement and innovative applications.

Figure 5. (a) Emission maxima and sizes of quantum dots of different composition. (Reprinted with permission from [54], copyright 2005 Science). (b) Typical structure of a quantum dots (QD) for biomedical applications. The core of the QD is passivated by a second semiconductor material. The core/shell QD is made hydrophilic and biocompatible by a polymer coating. The surface of the QD is conjugated with a targeting ligand for specific recognition and interaction with biological molecules. (c) Histology sections of lymph node (LN) 10 days post-injection: control regional auxiliary LN (RALN) (upper left), control right lateral thoracic LN (RLTLN) (lower left), RALN injected with QDs (upper right), and RLTLN injected with QDs (lower right). The lighter regions indicated with black arrows are the sites of inflammation. (d) Magnification of an inflammation area from RALN. There were many polynuclears observed but only some were indicated with blue arrows. Histiocytes (yellow arrows) and also vacuoles of digestion were also observed. (Reprinted with permission from [95], copyright 2009 Academy of Molecular Imaging).

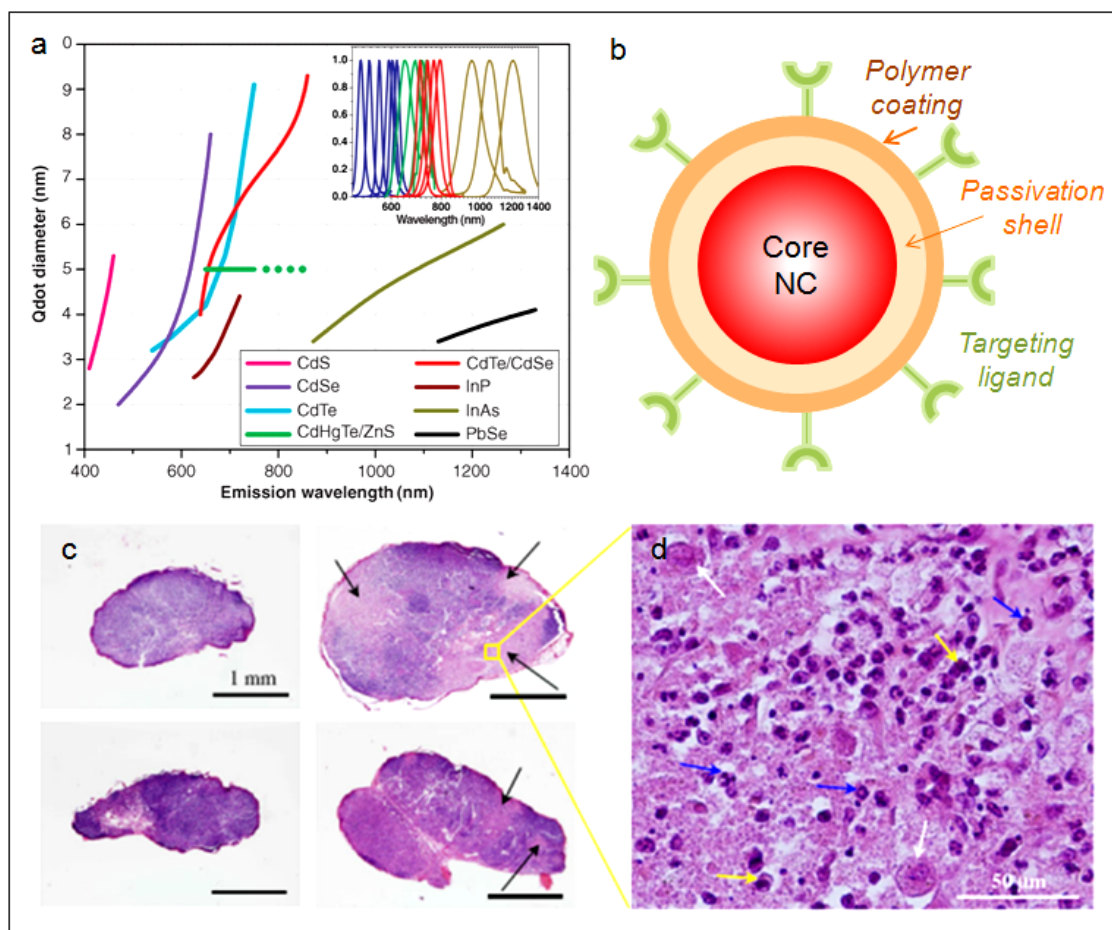
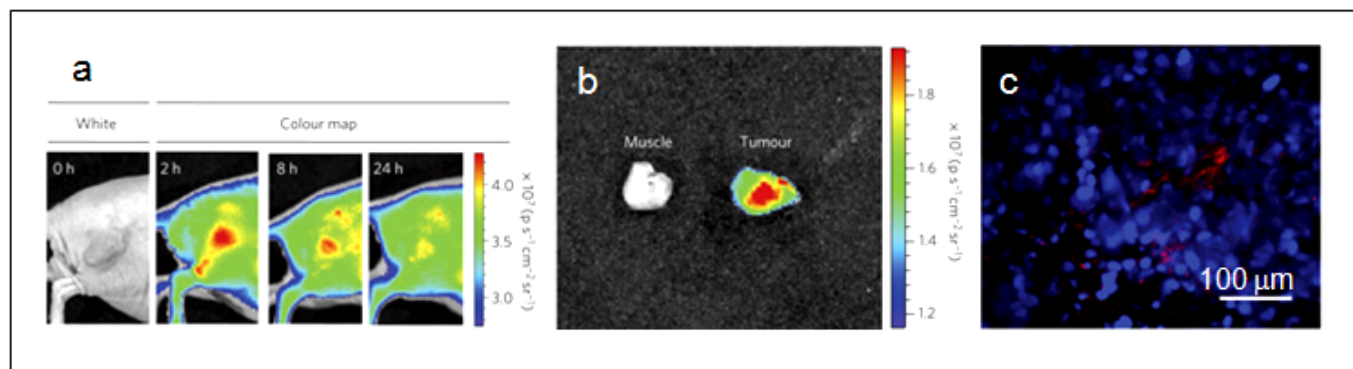


Figure 6. (a) Representative fluorescence images of a mouse with an MDA-MB-435 tumor. The mouse was imaged using a 615–665 nm excitation filter and an 810–875 nm emission filter at the indicated time post-intravenous injection of D-LPSiNPs (20 mg/kg). A strong signal from D-LPSiNPs is observed in the tumor, indicating significant passive accumulation in the tumor by the enhanced permeability and retention (EPR) effect. (b) *Ex vivo* fluorescence images of the tumor from the mouse used in (a). (c) Fluorescence images of a tumor slice from the mouse in (a). Red and blue indicate D-LPSiNPs and cell nuclei (DAPI stain). (Reprinted with permission from [99], copyright 2009 Macmillan).



4.3. Gold Nanoclusters

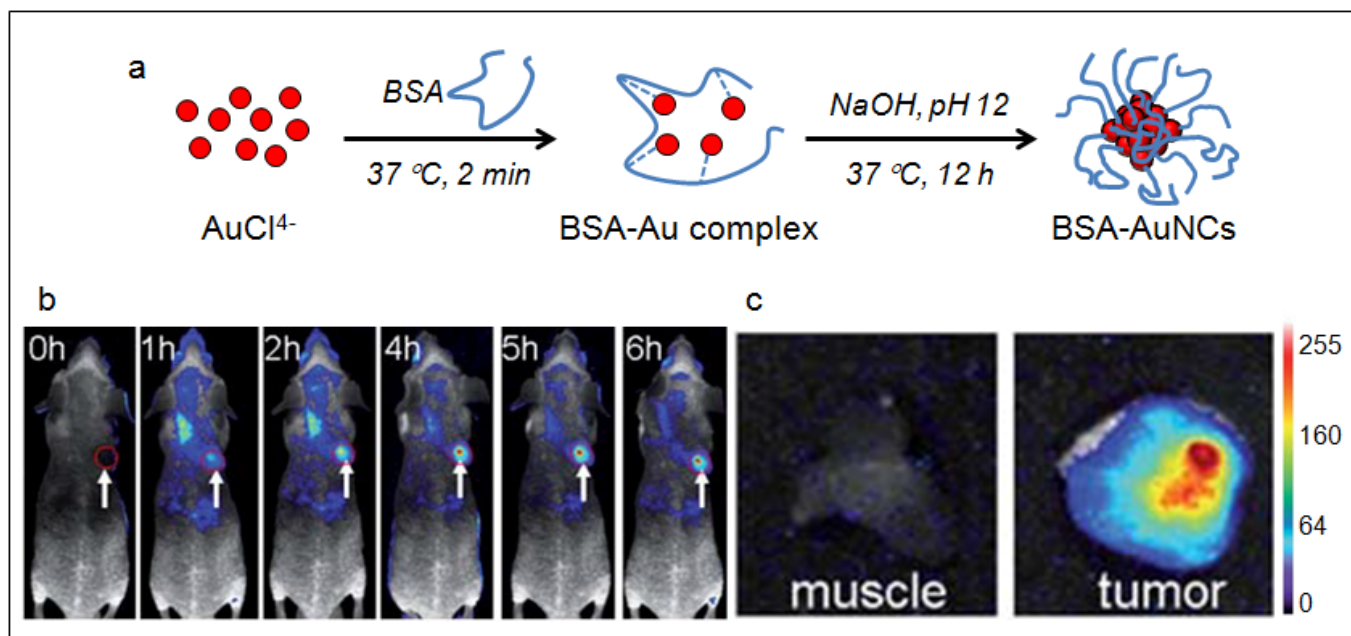
Fluorescence of noble metal nanoclusters (NCs) of gold and silver comprising of several to tens of atoms have drawn great attention in the past decade because of their remarkable optical properties [105–111]. Because of their minuscule size, high chemical stability and biocompatibility, NCs are increasingly being exploited for sensing [112–114], biolabeling [115,116] and bioimaging [117]. Typically, the size of NCs is less than 2 nm and their properties are governed by their subnanometer dimensions. Their size regime is intermediate of atomic and nanoparticles in which they no longer have plasmon resonance and Mie's theory is non-applicable [111]. In fact, the size of noble metal NCs is comparable to the Fermi wavelength of the conduction electrons, leading to molecule-like features such as discrete size-dependent electronic transitions, fluorescence and charging properties.

Multitudes of strategies have been developed for the synthesis of gold nanoclusters (AuNCs). One of which is chemical reduction of Au precursors in the presence of thiol stabilizers to afford AuNCs that fluoresce in the blue to near-IR regions [118–122]. However these NCs exhibit low quantum yields (QY) (0.001–0.1%). AuNCs can also be prepared via template-assisted synthesis within the cavities of dendrimers [111] with greater than 10% QY at the expense of fairly long reaction time of ~2 days along with the production of large nanoparticles (NPs) as byproduct. Another commonly used technique to prepare AuNCs is by ligand-induced core etching of metal NPs to yield blue-emission NCs [123]. Fine-tuning of the core etching method led Lin *et al.* to generate NIR AuNCs by first producing 6-nm diameter gold nanoparticles core stabilized with dihydrogenlipoic acid (DHLA) (AuNC@DHLA) [124,125]. Conjugation of AuNC@DHLA with biomolecules can easily be achieved with the carboxyl group on DHLA via carbodiimide chemistry. Polyethylene glycol (PEG, 5 kDa), PEG-biotin and avidin have been attached in this manner. The shortcoming of these NCs is the low quantum yield of 1–3%. Nevertheless, the authors demonstrated the specific labeling capability of the AuNCs toward fixed human hepatoma

cells (HepG₂) and also the non-specific uptake of the AuNCs by human aortic endothelial cells. The results make obvious that these AuNCs are relatively nontoxic.

With increasing interest in applying NIR fluorescent probes for bioimaging, effort has been devoted to developing biocompatible AuNCs via aqueous synthetic routes with biological molecules [126]. Xie *et al.* [127] has developed an innovative method by exploiting the reducing capability of bovine serum albumin (BSA) to prepare AuNCs consisted of 25 gold atoms with red emission [127]. The synthesis is similar to the biomineralization activities of organisms. Once added to aqueous BSA solution the Au ions were sequestered and entrapped within the protein molecules. The reduction ability of BSA was activated when the pH of the reaction was adjusted to ~12 and the ions were progressive reduced to AuNCs *in situ* (Figure 7a). Additional reductant, such as NaBH₄ would be required to yield AuNCs that emit at 683 nm. The quantum yield of the NIR AuNCs produced by this method was also low (0.1%). Despite that, Wu *et al.* demonstrated the applicability of these AuNCs for *in vivo* tumor fluorescence imaging using MSD-MB-45 and HeLa tumor xenograft models. They attributed the high accumulation of the NIR AuNCs in the tumor areas to the enhanced permeability and retention (EPR) effects (Figure 7b) [128].

Figure 7. (a) Schematic of the formation of AuNCs in BSA solution. (b) Fluorescence images of mice with a MDS-MB-45 tumor. Strong signal from AuNCs was observed in the tumor (red circle), indicating significant passive accumulation in the tumor by the EPR effect. White arrows indicate tumor site. (c) *Ex vivo* fluorescence image of the muscle and tumor tissue around the tumor from the mice used in b. (Reprinted with permission from [128], copyright 2010 The Royal Society of Chemistry).



5. Carbon Materials

5.1. Single-Walled Carbon Nanotubes

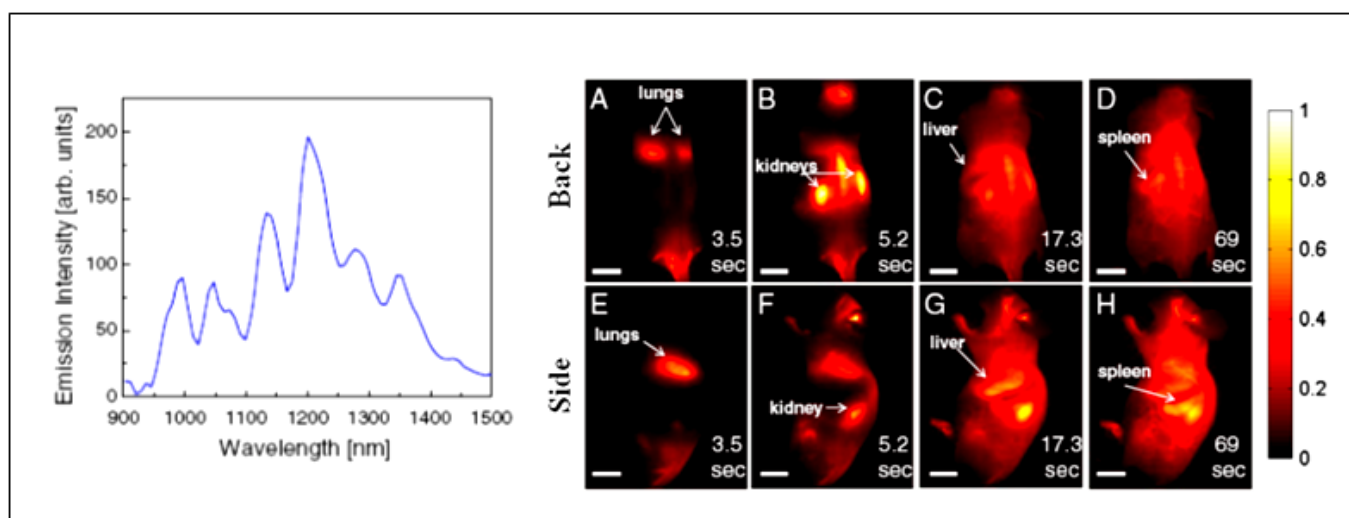
Carbon nanotubes (CNTs) represent another class of nanomaterials attract intense interest since their discovery in 1991 [129]. CNTs are cylindrical tubes of sp² carbon with superior optical, electrical, and

mechanical properties, thus have wide range of potential applications as nanoelectronics devices and engineered composite materials [48,49]. In addition, CNTs have been extensively explored as intracellular delivery vehicles for drugs, proteins and genes in cancer therapy [130,131].

CNTs are categorized as single-walled nanotubes (SWNTs) and multi-walled nanotubes (MWNTs). So far, only SWNTs have been reported to possess high emission in the NIR II region, making them suitable for deep-tissue *in vivo* imaging [132]. In general, SWNTs are most commonly synthesized by chemical vapor deposition that involves the heating of an alumina substrate with a layer of transition-metal catalytic nanoparticles, which serve as seeds to nucleate the growth of the nanotubes in a furnace with a stream of hydrocarbon gas flowing through the tube reactor [133]. SWNTs synthesized by this method have vast possibilities in the type of carbon tube “molecules”, giving rise to variation in band gaps ranging from ~ 10 meV to ~ 0.5 eV [133].

Welsher *et al.* suggested that the biggest obstacle in realizing the potential of SWNTs as NIR II probes is producing SWNTs with high quantum efficiency and good biocompatibility [132]. To overcome this issue, the authors came up with a strategy of first debundling and solubilizing the hydrophobic, pristine SWNTs in sodium cholate by sonification, followed by surfactant exchange to displace the sodium cholate with pegylated phospholipid (DSPE-mPEG). The resulting water-soluble SWNTs exhibit several emission peaks across the NIR II region when excited at 808 nm (Figure 8). When delivered into athymic nude mice via tail-vein injection, the systemic circulation and biodistribution of the SWNTs can be followed for over two minutes (Figure 8) [134]. This work shows the advantages of fluorescence imaging in the NIR II region and their potential impact in advancing nanomedicine.

Figure 8. *Left panel:* Fluorescence spectrum of DSPE-mPEG functionalized SWNTs excited at 808 nm, showing several emission peaks in the NIR II ranging from 1000–1400 nm. *Right panel:* Frames from video imaging of mice injected with SWNTs. At 3.5 s (A and E) post tail-vein injection, the lungs are the dominant feature, corresponding to flow of oxygen-poor, SWNT-rich blood to the lungs. At 5.3 s (B and F), the SWNT-rich blood flows through the highly vascularized kidney followed by the liver at 17.3 s (C and G) and the spleen at 69 s (D and H). (Reprinted with permission from [134], copyright 2011 PNAS).



6. Conclusion and Outlook

The potential of NIR fluorescent nanoprobe for *in vivo* application is unlimited. The drawbacks of organic dyes such as poor photostability, undesired aggregation and fluorescence in aqueous solution can be resolved by innovative NIR nanoprobe designs. In particular the versatile, nanomaterials-based NIR fluorescent probes offer ample opportunity to optimize their optical and targeting properties. Among all nanomaterial-based fluorescent probes, Si QDs is the only system that can be directly loaded with drugs and biodegraded into silicic acid that can be excreted efficiently through renal clearance. Like other nanomaterial-based fluorescent probes, improvement of their quantum efficiency, however, will still require significant effort. Robust and environmentally friendly synthetic routes that can produce these nanomaterials-based NIR nanoprobe with uniform size and colloidal stability represent other significant challenges. The widespread application of NIR fluorescent nanoprobe awaits demonstration of their long term biocompatibility, *in vivo* targeting efficacy as well as parallel development of advanced optical instrumentation for deep-tissue imaging capability. Nevertheless, their role in advancing the field of nanomedicine will undoubtedly be essential.

Acknowledgment

The authors would like to acknowledge funding through NIH (HL89764) and NSF EEC-0425626.

References

1. Kevles, B. *Naked to the Bone: Medical Imaging in the Twentieth Century*; Sloan Technology Series; Rutgers University Press: New Brunswick, NJ, Canada, 1997.
2. Rudin, M.; Weissleder, R. Molecular imaging in drug discovery and development. *Nat. Rev. Drug Discov.* **2003**, *2*, 123–131.
3. Massoud, T.F.; Gambhir, S.S. Molecular imaging in living subjects: Seeing fundamental biological processes in a new light. *Gene. Dev.* **2003**, *17*, 545–580.
4. Hargreaves, R.J. The role of molecular imaging in drug discovery and development. *Clin. Pharmacol. Ther.* **2008**, *83*, 349–353.
5. Weissleder, R. A clearer vision for *in vivo* imaging. *Nat. Biotechnol.* **2001**, *19*, 316–317.
6. Weissleder, R. Scaling down imaging: Molecular mapping of cancer in mice. *Nat. Rev. Cancer* **2002**, *2*, 11–18.
7. Contag, P.R. Whole-animal cellular and molecular imaging to accelerate drug development. *Drug Discov. Today* **2002**, *7*, 555–562.
8. Gross, S.; Piwnicka-Worms, D. Molecular imaging strategies for drug discovery and development. *Curr. Opin. Chem. Biol.* **2006**, *10*, 334–342.
9. Rudin, M. Noninvasive structural, functional, and molecular imaging in drug development. *Curr. Opin. Chem. Biol.* **2009**, *13*, 360–371.
10. Dufort, S.; Sancey, L.; Wenk, C.; Jossierand, V.; Coll, J.L. Optical small animal imaging in the drug discovery process. *BBA. Biomembranes* **2010**, *1798*, 2266–2273.
11. Sivaraman, D.; Biswas, P.; Cella, L.N.; Yates, M.V.; Chen, W. Detecting RNA viruses in living mammalian cells by fluorescence microscopy. *Trends Biotech.* **2011**, *29*, 307–313.

12. Koba, W.; Kim, K.; Lipton, M.L.; Jelicks, L.; Das, B.; Herbst, L.; Fine, E. Imaging devices for use in small animals. *Semin. Nucl. Med.* **2011**, *41*, 151–165.
13. Hickson, J. *In vivo* optical imaging: Preclinical applications and considerations. *Urol. Oncol. Semin. Orig. Investi.* **2009**, *27*, 295–297.
14. Frangioni, J.V. *In vivo* near-infrared fluorescence imaging. *Curr. Opin. Chem. Biol.* **2003**, *7*, 626–634.
15. Smith, A.M.; Mancini, M.C.; Nie, S.M. BIOIMAGING: Second window for *in vivo* imaging. *Nat. Nanotechnol.* **2009**, *4*, 710–711.
16. Gioux, S.; Choi, H.S.; Frangioni, J.V. Image-guided surgery using invisible near-infrared light: Fundamentals of clinical translation. *Mol. Imaging* **2010**, *9*, 237–255.
17. Schaafsma, B.E.; Mieog, J.S.D.; Hutteman, M.; van der Vorst, J.R.; Kuppen, P.J.K.; Lowik, C.; Frangioni, J.V.; van de Velde, C.J.H.; Vahrmeijer, A.L. The clinical use of indocyanine green as a near-infrared fluorescent contrast agent for image-guided oncologic surgery. *J. Surg. Oncol.* **2011**, *104*, 323–332.
18. Mishra, A.; Behera, R.K.; Behera, P.K.; Mishra, B.K.; Behera, G.B. Cyanines during the 1990s: A review. *Chem.Rev.* **2000**, *100*, 1973–2011.
19. Licha, K. Contrast agents for optical imaging. In *Contrast Agents II*; Krause, W., Ed.; Springer-Verlag: Berlin, Germany, 2002; pp. 1–29.
20. Kim, D.E.; Jaffer, F.A.; Weissleder, R.; Tung, C.H.; Schellingerhout, D. Near-infrared fluorescent imaging of cerebral thrombi and blood-brain barrier disruption in a mouse model of cerebral venous sinus thrombosis. *J. Cerebr. Blood Flow Metabol.* **2005**, *25*, 226–233.
21. Liu, X.; Guo, X.L.; Liu, F.; Zhang, Y.; Zhang, H.; Hu, G.S.; Bai, J. Imaging of indocyanine green perfusion in mouse liver with fluorescence diffuse optical tomography. *IEEE Trans. Biomed. Eng.* **2011**, *58*, 2139–2143.
22. Herbort, C.P.; LeHoang, P.; Guex-Crosier, Y. Schematic interpretation of indocyanine green angiography in posterior uveitis using a standard angiographic protocol. *Ophthalmology* **1998**, *105*, 432–440.
23. Achilefu, S.; Dorshow, R.B. Dynamic and continuous monitoring of renal and hepatic functions with exogenous markers. *Contrast Agent. II* **2002**, *222*, 31–72.
24. Liebert, A.; Wabnitz, H.; Obrig, H.; Erdmann, R.; Moller, M.; Macdonald, R.; Rinneberg, H.; Villringer, A.; Steinbrink, J. Non-invasive detection of fluorescence from exogenous chromophores in the adult human brain. *Neuroimage* **2006**, *31*, 600–608.
25. Liebert, A.; Sawosz, P.; Milej, D.; Kacprzak, M.; Weigl, W.; Botwicz, M.; Maczewska, J.; Fronczewska, K.; Mayzner-Zawadzka, E.; Krolicki, L.; Maniewski, R. Assessment of inflow and washout of indocyanine green in the adult human brain by monitoring of diffuse reflectance at large source-detector separation. *J. Biomed. Opt.* **2011**, *16*, 046011.
26. Yamamoto, M.; Sasaguri, S.; Sato, T. Assessing intraoperative blood flow in cardiovascular surgery. *Surg. Today* **2011**, *41*, 1467–1474.
27. Raabe, A.; Beck, J.; Gerlach, R.; Zimmermann, M.; Seifert, V. Near-infrared indocyanine green video angiography: A new method for intraoperative assessment of vascular flow. *Neurosurgery* **2003**, *52*, 132–139.

28. Taggart, D.P.; Choudhary, B.; Anastasiadis, K.; Abu-Omar, Y.; Balacumaraswami, L.; Pigott, D.W. Preliminary experience with a novel intraoperative fluorescence imaging technique to evaluate the patency of bypass grafts in total arterial revascularization. *Ann. Thorac. Surg.* **2003**, *75*, 870–873.
29. Folli, S.; Westermann, P.; Braichotte, D.; Pelegrin, A.; Wagnieres, G.; Vandenberg, H.; Mach, J.P. Antibody-indocyanin conjugates for immunophotodetection of human squamous-cell carcinoma in nude-mice. *Cancer Res.* **1994**, *54*, 2643–2649.
30. Ballou, B.; Fisher, G.W.; Waggoner, A.S.; Farkas, D.L.; Reiland, J.M.; Jaffe, R.; Mujumdar, R.B.; Mujumdar, S.R.; Hakala, T.R. Tumor labeling *in-vivo* using cyanine-conjugated monoclonal-antibodies. *Cancer Immunol. Immunother.* **1995**, *41*, 257–263.
31. Ballou, B.; Fisher, G.W.; Hakala, T.R.; Farkas, D.L. Tumor detection and visualization using cyanine fluorochrome-labeled antibodies. *Biotechnol. Progr.* **1997**, *13*, 649–658.
32. Neri, D.; Carnemolla, B.; Nissim, A.; Leprini, A.; Querze, G.; Balza, E.; Pini, A.; Tarli, L.; Halin, C.; Neri, P.; Zardi, L.; Winter, G. Targeting by affinity-matured recombinant antibody fragments of an angiogenesis associated fibronectin isoform. *Nat. Biotechnol.* **1997**, *15*, 1271–1275.
33. Birchler, M.; Neri, G.; Tarli, L.; Halin, C.; Viti, F.; Neri, D. Infrared photodetection for the *in vivo* localisation of phage-derived antibodies directed against angiogenic markers. *J. Immunol. Method.* **1999**, *231*, 239–248.
34. Bugaj, J.E.; Achilefu, S.; Dorshow, R.B.; Rajagopalan, R. Novel fluorescent contrast agents for optical imaging of *in vivo* tumors based on a receptor-targeted dye-peptide conjugate platform. *J. Biomed. Opt.* **2001**, *6*, 122–133.
35. Achilefu, S.; Jimenez, H.N.; Dorshow, R.B.; Bugaj, J.E.; Webb, E.G.; Wilhelm, R.R.; Rajagopalan, R.; Jöhler, J.; Erion, J.L. Synthesis, *in vitro* receptor binding, and *in vivo* evaluation of fluorescein and carbocyanine peptide-based optical contrast agents. *J. Med. Chem.* **2002**, *45*, 2003–2015.
36. Becker, A.; Hassenius, C.; Licha, K.; Ebert, B.; Sukowski, U.; Semmler, W.; Wiedenmann, B.; Grotzinger, C. Receptor-targeted optical imaging of tumors with near-infrared fluorescent ligands. *Nat. Biotechnol.* **2001**, *19*, 327–331.
37. Weissleder, R.; Tung, C.H.; Mahmood, U.; Bogdanov, A. *In vivo* imaging of tumors with protease-activated near-infrared fluorescent probes. *Nat. Biotechnol.* **1999**, *17*, 375–378.
38. Bullock, K.E.; Maxwell, D.; Kesarwala, A.H.; Gammon, S.; Prior, J.L. Snow, M.; Stanley, S.; Piwnicka-Worms, D. Biochemical and *in vivo* characterization of a small, membrane-permeant, caspase-activatable far-red fluorescent peptide for imaging apoptosis. *Biochemistry* **2007**, *46*, 4055–4065.
39. Edgington, L.E.; Berger, A.B.; Blum, G.; Albrow, V.E.; Paulick, M.G.; Lineberry, N.; Bogoy, M. Noninvasive optical imaging of apoptosis by caspase-targeted activity-based probes. *Nature Med.* **2009**, *15*, 967–973.
40. Bremer, C.; Ntziachristos, V.; Weissleder, R. Optical-based molecular imaging: Contrast agents and potential medical applications. *European Radiol.* **2003**, *13*, 231–243.
41. Figueiredo, J.L.; Alencar, H.; Weissleder, R.; Mahmood, U. Near infrared thoracoscopy of tumoral protease activity for improved detection of peripheral lung cancer. *Int. J. Cancer* **2006**, *118*, 2672–2677.

42. Blum, G.; von Degenfeld, G.; Merchant, M.J.; Blau, H.M.; Bogoyo, M. Noninvasive optical imaging of cysteine protease activity using fluorescently quenched activity-based probes. *Nat. Chem. Biol.* **2007**, *3*, 668–677.
43. Weissleder, R.; Ntziachristos, V. Shedding light onto live molecular targets. *Nature Med.* **2003**, *9*, 123–128.
44. Marten, K.; Bremer, C.; Khazaie, K.; Sameni, M.; Sloane, B.; Tung, C.H.; Weissleder, R. Detection of dysplastic intestinal adenomas using enzyme-sensing molecular beacons in mice. *Gastroenterology* **2002**, *122*, 406–414.
45. Escobedo, J.O.; Rusin, O.; Lim, S.; Strongin, R.M. NIR dyes for bioimaging applications. *Curr. Opin. Chem. Biol.* **2010**, *14*, 64–70.
46. Lordi, V.; Yao, N.; Wei, J. Method for supporting platinum on single-walled carbon nanotubes for a selective hydrogenation catalyst. *Chem. Mater.* **2001**, *13*, 733–737.
47. Huynh, W.U.; Dittmer, J.J.; Alivisatos, A.P. Hybrid nanorod-polymer solar cells. *Science* **2002**, *295*, 2425–2427.
48. Baughman, R.H.; Zakhidov, A.A.; de Heer, W.A. Carbon nanotubes—The route toward applications. *Science* **2002**, *297*, 787–792.
49. Fischer, J.E.; Dai, H.; Thess, A.; Lee, R.; Hanjani, N.M.; Dehaas, D.L.; Smalley, R.E. Metallic resistivity in crystalline ropes of single-wall carbon nanotubes. *Phys. Rev. B* **1997**, *55*, R4921–R4924.
50. Porti, M.; Blasco, X.; Nafria, M.; Aymerich, X. Electrical characterization and fabrication of SiO₂ based metal-oxide-semiconductor nanoelectronic devices with atomic force microscopy. *Nanotechnology* **2003**, *14*, 584–587.
51. Roduner, E. Size matters: Why nanomaterials are different. *Chem. Soc. Rev.* **2006**, *35*, 583–592.
52. Buhro, W.E.; Colvin, V.L. Semiconductor nanocrystals—Shape matters. *Nat. Mater.* **2003**, *2*, 138–139.
53. Bruchez, M.; Moronne, M.; Gin, P.; Weiss, S.; Alivisatos, A.P. Semiconductor nanocrystals as fluorescent biological labels. *Science* **1998**, *281*, 2013–2016.
54. Michalet, X.; Pinaud, F.F.; Bentolila, L.A.; Tsay, J.M.; Doose, S.; Li, J.J.; Sundaresan, G.; Wu, A.M.; Gambhir, S.S.; Weiss, S. Quantum dots for live cells, *in vivo* imaging, and diagnostics. *Science* **2005**, *307*, 538–544.
55. Alivisatos, P. The use of nanocrystals in biological detection. *Nat. Biotechnol.* **2004**, *22*, 47–52.
56. Chan, W.C.W.; Maxwell, D.J.; Gao, X.H.; Bailey, R.E.; Han, M.Y.; Nie, S.M. Luminescent quantum dots for multiplexed biological detection and imaging. *Curr. Opin. Biotechnol.* **2002**, *13*, 40–46.
57. Medintz, I.L.; Uyeda, H.T.; Goldman, E.R.; Mattoussi, H. Quantum dot bioconjugates for imaging, labelling and sensing. *Nat. Mater.* **2005**, *4*, 435–446.
58. Clarke, S.J.; Hollmann, C.A.; Zhang, Z.J.; Suffern, D.; Bradforth, S.E.; Dimitrijevic, N.M.; Minarik, W.G.; Nadeau, J.L. Photophysics of dopamine-modified quantumdots and effects on biological systems. *Nat. Mater.* **2006**, *5*, 409–417.
59. Li, J.B.; Wu, D.D.; Miao, Z.R.; Zhang, Y. Preparation of quantum dot bioconjugates and their applications in bio-imaging. *Curr. Pharm. Biotechnol.* **2010**, *11*, 662–671.

60. Dubertret, B.; Skourides, P.; Norris, D.J.; Noireaux, V.; Brivanlou, A.H.; Libchaber, A. *In vivo* imaging of quantum dots encapsulated in phospholipid micelles. *Science* **2002**, *298*, 1759–1762.
61. Gao, X.H.; Cui, Y.Y.; Levenson, R.M.; Chung, L.W.K.; Nie, S.M. *In vivo* cancer targeting and imaging with semiconductor quantum dots. *Nat. Biotechnol.* **2004**, *22*, 969–976.
62. Derfus, A.M.; Chen, A.A.; Min, D.H.; Ruoslahti, E.; Bhatia, S.N. Targeted quantum dot conjugates for siRNA delivery. *Bioconjug. Chem.* **2007**, *18*, 1391–1396.
63. Tan, W.B.; Jiang, S.; Zhang, Y. Quantum-dot based nanoparticles for targeted silencing of HER2/neu gene *via* RNA interference. *Biomaterials* **2007**, *28*, 1565–1571.
64. Lee, H.; Kim, I.K.; Park, T.G. Intracellular trafficking and unpacking of siRNA/quantum dot-PEI complexes modified with and without cell penetrating peptide: Confocal and flow cytometric FRET analysis. *Bioconjug. Chem.* **2010**, *21*, 289–295.
65. Hong, H.; Zhang, Y.; Cai, W.B. *In vivo* imaging of RNA interference. *J. Nucl. Med.* **2010**, *51*, 169–172.
66. Clapp, A.R.; Medintz, I.L.; Mattoussi, H. Forster resonance energy transfer investigations using quantum-dot fluorophores. *ChemPhysChem* **2006**, *7*, 47–57.
67. Chen, H.H.; Leong, K.W. Quantum-dots-FRET nanosensors for detecting unamplified nucleic acids by single molecule detection. *Nanomedicine* **2006**, *1*, 119–122.
68. Ho, Y.P.; Chen, H.H.; Leong, K.W.; Wang, T.H. Evaluating the intracellular stability and unpacking of DNA nanocomplexes by quantum dots-FRET. *J. Control. Release* **2006**, *116*, 83–89.
69. Chen, H.H.; Ho, Y.P.; Jiang, X.; Mao, H.Q.; Wang, T.H.; Leong, K.W. Quantitative comparison of intracellular unpacking kinetics of polyplexes by a model constructed from quantum Dot-FRET. *Mol. Ther.* **2008**, *16*, 324–332.
70. Rieger, S.; Kulkarni, R.P.; Darcy, D.; Fraser, S.E.; Koster, R.W. Quantum dots are powerful multipurpose vital labeling agents in zebrafish embryos. *Dev. Dynam.* **2005**, *234*, 670–681.
71. Slotkin, J.R.; Chakrabarti, L.; Dai, H.N.; Carney, R.S.E.; Hirata, T.; Bregman, B.S.; Gallicano, G.I.; Corbin, J.G.; Haydar, T.F. *In vivo* quantum dot labeling of mammalian stem and progenitor cells. *Dev. Dynam.* **2007**, *236*, 3393–3401.
72. Gaponik, N.; Rogach, A.L. Thiol-capped CdTe nanocrystals: Progress and perspectives of the related research fields. *PCCP Phys. Chem. Chem. Phys.* **2010**, *12*, 8685–8693.
73. Zintchenko, A.; Susha, A.S.; Concia, M.; Feldmann, J.; Wagner, E.; Rogach, A.L.; Ogris, M. Drug nanocarriers labeled with near-infrared-emitting quantum dots (quantoplexes): Imaging fast dynamics of distribution in living animals. *Mol. Ther.* **2009**, *17*, 1849–1856.
74. Kim, S.; Lim, Y.T.; Soltesz, E.G.; De Grand, A.M.; Lee, J.; Nakayama, A.; Parker, J.A.; Mihaljevic, T.; Laurence, R.G.; Dor, D.M.; Cohn, L.H.; Bawendi, M.G.; Frangioni, J.V. Near-infrared fluorescent type II quantum dots for sentinel lymph node mapping. *Nat. Biotechnol.* **2004**, *22*, 93–97.
75. Tsay, J.M.; Pflughoefft, M.; Bentolila, L.A.; Weiss, S. Hybrid approach to the synthesis of highly luminescent CdTe/ZnS and CdHgTe/ZnS nanocrystals. *J. Am. Chem. Soc.* **2004**, *126*, 1926–1927.
76. Rogach, A.L.; Harrison, M.T.; Kershaw, S.V.; Kornowski, A.; Burt, M.G.; Eychmuller, A.; Weller, H. Colloidally prepared CdHgTe and HgTe quantum dots with strong near-infrared luminescence. *Phys. Status Solid B Basic Re.* **2001**, *224*, 153–158.

77. Zimmer, J.P.; Kim, S.W.; Ohnishi, S.; Tanaka, E.; Frangioni, J.V.; Bawendi, M.G. Size series of small indium arsenide-zinc selenide core-shell nanocrystals and their application to *in vivo* imaging. *J. Am. Chem. Soc.* **2006**, *128*, 2526–2527.
78. Kim, S.W.; Zimmer, J.P.; Ohnishi, S.; Tracy, J.B.; Frangioni, J.V.; Bawendi, M.G. Engineering InAs_xP_{1-x}/InP/ZnSe III-V alloyed core/shell quantum dots for the near-infrared. *J. Am. Chem. Soc.* **2005**, *127*, 10526–10532.
79. Jasieniak, J.; Califano, M.; Watkins, S.E. Size-dependent valence and conduction band-edge energies of semiconductor nanocrystals. *ACS Nano* **2011**, *5*, 5888–5902.
80. Dai, Q.Q.; Wang, Y.N.; Li, X.B.; Zhang, Y.; Pellegrino, D.J.; Zhao, M.X.; Zou, B.; Seo, J.; Wang, Y.D.; Yu, W.W. Size-dependent composition and molar extinction coefficient of PbSe semiconductor nanocrystals. *ACS Nano* **2009**, *3*, 1518–1524.
81. Derfus, A.M.; Chan, W.C.W.; Bhatia, S.N. Probing the cytotoxicity of semiconductor quantum dots. *Nano Lett.* **2004**, *4*, 11–18.
82. Guo, G.N.; Liu, W.; Liang, J.G.; He, Z.K.; Xu, H.B.; Yang, X.L. Probing the cytotoxicity of CdSe quantum dots with surface modification. *Mater. Lett.* **2007**, *61*, 1641–1644.
83. Cho, S.J.; Maysinger, D.; Jain, M.; Roder, B.; Hackbarth, S.; Winnik, F.M. Long-term exposure to CdTe quantum dots causes functional impairments in live cells. *Langmuir* **2007**, *23*, 1974–1980.
84. Hardman, R. A toxicologic review of quantum dots: Toxicity depends on physicochemical and environmental factors. *Environ. Health Perspect.* **2006**, *114*, 65–172.
85. Kirchner, C.; Liedl, T.; Kudera, S.; Pellegrino, T.; Javier, A.M.; Gaub, H.E.; Stolzle, S.; Fertig, N.; Parak, W.J. Cytotoxicity of colloidal CdSe and CdSe/ZnS nanoparticles. *Nano Lett.* **2005**, *5*, 331–338.
86. Xie, R.G.; Peng, X.G. Synthesis of Cu-doped InP nanocrystals (d-dots) with ZnSe diffusion barrier as efficient and color-tunable NIR emitters. *J. Am. Chem. Soc.* **2009**, *131*, 10645–10651.
87. Allen, P.M.; Bawendi, M.G. Ternary I-III-VI quantum dots luminescent in the red to near-infrared. *J. Am. Chem. Soc.* **2008**, *130*, 9240–9241.
88. Park, J.; Dvoracek, C.; Lee, K.H.; Galloway, J.F.; Bhang, H.E.C.; Pomper, M.G.; Searson, P.C. CuInSe/ZnS Core/Shell NIR quantum dots for biomedical imaging. *Small* **2011**, *7*, 3148–3152.
89. Zhang, W.J.; Zhong, X.H. Facile synthesis of ZnS-CuInS(2)-alloyed nanocrystals for a color-tunable fluorochrome and photocatalyst. *Inorg. Chem.* **2011**, *50*, 4065–4072.
90. Pons, T.; Pic, E.; Lequeux, N.; Cassette, E.; Bezdetnaya, L.; Guillemin, F.; Marchal, F.; Dubertret, B. Cadmium-free CuInS(2)/ZnS quantum dots for sentinel lymph node imaging with reduced toxicity. *ACS Nano* **2010**, *4*, 2531–2538.
91. Smith, A.M.; Dave, S.; Nie, S.M.; True, L.; Gao, X.H. Multicolor quantum dots for molecular diagnostics of cancer. *Expert Rev. Mol. Diagn.* **2006**, *6*, 231–244.
92. Alivisatos, A.P.; Gu, W.W.; Larabell, C. Quantum dots as cellular probes. *Ann. Rev. Biomed. Eng.* **2005**, *7*, 55–76.
93. Uyeda, H.T.; Medintz, I.L.; Jaiswal, J.K.; Simon, S.M.; Mattoussi, H. Synthesis of compact multidentate ligands to prepare stable hydrophilic quantum dot fluorophores. *J. Am. Chem. Soc.* **2005**, *127*, 3870–3878.

94. Carion, O.; Mahler, B.; Pons, T.; Dubertret, B. Synthesis, encapsulation, purification and coupling of single quantum dots in phospholipid micelles for their use in cellular and *in vivo* imaging. *Nat. Protoc.* **2007**, *2*, 2383–2390.
95. Pic, E.; Pons, T.; Bezdetnaya, L.; Leroux, A.; Guillemin, F.; Dubertret, B.; Marchall, F. Fluorescence imaging and whole-body biodistribution of near-infrared-emitting quantum dots after subcutaneous injection for regional lymph node mapping in mice. *Mol. Imaging Biol.* **2010**, *12*, 394–405.
96. Vogel, E.M. Technology and metrology of new electronic materials and devices. *Nat. Nanotechnol.* **2007**, *2*, 25–32.
97. Melinon, P.; Masenelli, B.; Tournus, F.; Perez, A. Playing with carbon and silicon at the nanoscale. *Nat. Mater.* **2007**, *6*, 479–490.
98. Fujioka, K.; Hiruoka, M.; Sato, K.; Manabe, N.; Miyasaka, R.; Hanada, S.; Hoshino, A.; Tilley, R.D.; Manome, Y.; Hirakuri, K.; Yamamoto, K. Luminescent passive-oxidized silicon quantum dots as biological staining labels and their cytotoxicity effects at high concentration. *Nanotechnology* **2008**, *19*, 415102.
99. Park, J.H.; Gu, L.; von Maltzahn, G.; Ruoslahti, E.; Bhatia, S.N.; Sailor, M.J. Biodegradable luminescent porous silicon nanoparticles for *in vivo* applications. *Nat. Mater.* **2009**, *8*, 331–336.
100. Erogbogbo, F.; Yong, K.T.; Roy, I.; Xu, G.X.; Prasad, P.N.; Swihart, M.T. Biocompatible luminescent silicon quantum dots for imaging of cancer cells. *ACS Nano* **2008**, *2*, 873–878.
101. Erogbogbo, F.; Yong, K.T.; Hu, R.; Law, W.C.; Ding, H.; Chang, C.W.; Prasad, P.N.; Swihart, M.T. Biocompatible magnetofluorescent probes: Luminescent silicon quantum dots coupled with superparamagnetic iron(III) oxide. *ACS Nano* **2010**, *4*, 5131–5138.
102. Li, X.G.; He, Y.Q.; Talukdar, S.S.; Swihart, M.T. Process for preparing macroscopic quantities of brightly photoluminescent silicon nanoparticles with emission spanning the visible spectrum. *Langmuir* **2003**, *19*, 8490–8496.
103. Hua, F.J.; Erogbogbo, F.; Swihart, M.T.; Ruckenstein, E. Organically capped silicon nanoparticles with blue photoluminescence prepared by hydrosilylation followed by oxidation. *Langmuir* **2006**, *22*, 4363–4370.
104. Li, Z.F.; Ruckenstein, E. Water-soluble poly(acrylic acid) grafted luminescent silicon nanoparticles and their use as fluorescent biological staining labels. *Nano Lett.* **2004**, *4*, 1463–1467.
105. Sun, Y.; Balasubramanian, K.; Rao, T.U.B.; Pradeep, T. First principles studies of two luminescent molecular quantum clusters of silver, Ag(7)(H(2)MSA)(7) and Ag(8)(H(2)MSA)(8), based on experimental fluorescence spectra. *J. Phys. Chem. C* **2011**, *115*, 20380–20387.
106. Yuan, X.; Luo, Z.T.; Zhang, Q.B.; Zhang, X.H.; Zheng, Y.G.; Lee, J.Y.; Xie, J.P. Synthesis of highly fluorescent metal (Ag, Au, Pt, and Cu) nanoclusters by electrostatically induced reversible phase transfer. *ACS Nano* **2011**, *5*, 8800–8808.
107. Selvam, T.S.; Chi, K.M. Synthesis of hydrophobic gold nanoclusters: Growth mechanism study, luminescence property and catalytic application. *J. Nanopart. Res.* **2011**, *13*, 1769–1780.
108. Devadas, M.S.; Kim, J.; Sinn, E.; Lee, D.; Goodson, T.; Ramakrishna, G. Unique ultrafast visible luminescence in monolayer-protected Au(25) clusters. *J. Phys. Chem. C* **2010**, *114*, 22417–22423.
109. Wu, Z.K.; Jin, R.C. On the ligand's role in the fluorescence of gold nanoclusters. *Nano Lett.* **2010**, *10*, 2568–2573.

110. Guo, S.J.; Wang, E.K. Noble metal nanomaterials: Controllable synthesis and application in fuel cells and analytical sensors. *Nano Today* **2011**, *6*, 240–264.
111. Zheng, J.; Nicovich, P.R.; Dickson, R.M. Highly fluorescent noble-metal quantum dots, in Annual Review of Physical Chemistry. *Annu. Rev. Phys. Chem.* **2007**, *58*, 409–431.
112. Shang, L.; Dong, S.J. Sensitive detection of cysteine based on fluorescent silver clusters. *Biosens. Bioelectron.* **2009**, *24*, 1569–1573.
113. Huang, C.C.; Chen, C.T.; Shiang, Y.C.; Lin, Z.H.; Chang, H.T. Synthesis of fluorescent carbohydrate-protected Au nanodots for detection of concanavalin A and escherichia coli. *Anal. Chem.* **2009**, *81*, 875–882.
114. Wei, H.; Wang, Z.D.; Yang, L.M.; Tian, S.L.; Hou, C.J.; Lu, Y. Lysozyme-stabilized gold fluorescent cluster: Synthesis and application as Hg(2+) sensor. *Analyst* **2010**, *135*, 1406–1410.
115. Yu, J.; Patel, S.A.; Dickson, R.M. *In vitro* and intracellular production of peptide-encapsulated fluorescent silver nanoclusters. *Angew. Chem. Int. Ed.* **2007**, *46*, 2028–2030.
116. Richards, C.I.; Choi, S.; Hsiang, J.C.; Antoku, Y.; Vosch, T. Bongiorno, A.; Tzeng, Y.L.; Dickson, R.M. Oligonucleotide-stabilized Ag nanocluster fluorophores. *J. Am. Chem. Soc.* **2008**, *130*, 5038–5039.
117. Yu, J.H.; Choi, S.; Dickson, R.M. Shuttle-based fluorogenic silver-cluster biolabels. *Angew. Chem. Int. Ed.* **2009**, *48*, 318–320.
118. Negishi, Y.; Takasugi, Y.; Sato, S.; Yao, H.; Kimura, K.; Tsukuda, T. Magic-numbered Au-*n* clusters protected by glutathione monolayers (*n* = 18, 21, 25, 28, 32, 39): Isolation and spectroscopic characterization. *J. Am. Chem. Soc.* **2004**, *126*, 6518–6519.
119. Negishi, Y.; Nobusada, K.; Tsukuda, T. Glutathione-protected gold clusters revisited: Bridging the gap between gold(I)-thiolate complexes and thiolate-protected gold nanocrystals. *J. Am. Chem. Soc.* **2005**, *127*, 5261–5270.
120. Negishi, Y.; Chaki, N.K.; Shichibu, Y.; Whetten, R.L.; Tsukuda, T. Origin of magic stability of thiolated gold clusters: A case study on Au-25(SC₆H₁₃)(18). *J. Am. Chem. Soc.* **2007**, *129*, 11322–11323.
121. Wang, G.L.; Huang, T.; Murray, R.W.; Menard, L.; Nuzzo, R.G. Near-IR luminescence of monolayer-protected metal clusters. *J. Am. Chem. Soc.* **2005**, *127*, 812–813.
122. Shichibu, Y.; Negishi, Y.; Tsunoyama, H.; Kanehara, M.; Teranishi, T. Tsukuda, T. Extremely high stability of glutathionate-protected Au-25 clusters against core etching. *Small* **2007**, *3*, 835–839.
123. Duan, H.W.; Nie, S.M. Etching colloidal gold nanocrystals with hyperbranched and multivalent polymers: A new route to fluorescent and water-soluble atomic clusters. *J. Am. Chem. Soc.* **2007**, *129*, 2412–2413.
124. Jana, N.R.; Peng, X.G. Single-phase and gram-scale routes toward nearly monodisperse Au and other noble metal nanocrystals. *J. Am. Chem. Soc.* **2003**, *125*, 14280–14281.
125. Lin, C.A.J.; Yang, T.Y.; Lee, C.H.; Huang, S.H.; Sperling, R.A.; Zanella, M.; Li, J.K.; Shen, J.L.; Wang, H.H.; Yeh, H.I.; Parak, W.J.; Chang, W.H. Synthesis, characterization, and bioconjugation of fluorescent gold nanoclusters toward biological labeling applications. *ACS Nano* **2009**, *3*, 395–401.

126. Bao, Y.; Yeh, H.C.; Zhong, C.; Ivanov, S.A.; Sharma, J.K.; Neidig, M.L.; Vu, D.M.; Shreve, A.P.; Dyer, R.B.; Werner, J.H.; Martinez, J.S. Formation and stabilization of fluorescent gold nanoclusters using small molecules. *J. Phys. Chem. C* **2010**, *114*, 15879–15882.
127. Xie, J.P.; Zheng, Y.G.; Ying, J.Y. Protein-directed synthesis of highly fluorescent gold nanoclusters. *J. Am. Chem. Soc.* **2009**, *131*, 888–889.
128. Wu, X.; He, X.; Wang, K.; Xie, C.; Zhou, B.; Qing, Z. Ultrasmall near-infrared gold nanoclusters for tumor fluorescence imaging *in vivo*. *Nanoscale* **2010**, *2*, 2244–2249.
129. Iijima, S. Helical microtubules of graphitic carbon. *Nature* **1991**, *354*, 56–58.
130. Feng, L.Z.; Liu, Z.A. Graphene in biomedicine: opportunities and challenges. *Nanomedicine* **2011**, *6*, 317–324.
131. Liu, Z.; Robinson, J.T.; Tabakman, S.M.; Yang, K.; Dai, H.J. Carbon materials for drug delivery & cancer therapy. *Mater. Today* **2011**, *14*, 316–323.
132. Welsher, K.; Liu, Z.; Sherlock, S.P.; Robinson, J.T.; Chen, Z.; Daranciang, D.; Dai, H.J. A route to brightly fluorescent carbon nanotubes for near-infrared imaging in mice. *Nat. Nanotechnol.* **2009**, *4*, 773–780.
133. Dai, H.J. Carbon nanotubes: Synthesis, integration, and properties. *Account. Chem. Res.* **2002**, *35*, 1035–1044.
134. Welsher, K.; Sherlock, S.P.; Dai, H.J. Deep-tissue anatomical imaging of mice using carbon nanotube fluorophores in the second near-infrared window. *Proc. Nat. Acad. Sci. USA* **2011**, *108*, 8943–8948.

© 2012 by the authors; licensee MDPI, Basel, Switzerland. This article is an open access article distributed under the terms and conditions of the Creative Commons Attribution license (<http://creativecommons.org/licenses/by/3.0/>).